Published OnlineFirst July 28, 2017; DOI: 10.1158/1078-0432.CCR-16-1217

Cancer Therapy: Preclinical

Clinical Cancer Research

Multifaceted Role of BTLA in the Control of CD8$^+$ T-cell Fate after Antigen Encounter

Krit Ritthipichai[1,2], Cara L. Haymaker[1], Melisa Martinez[3], Andrew Aschenbrenner[4], Xiaohui Yi[5], Minying Zhang[1], Charuta Kale[1], Luis M. Vence[5], Jason Roszik[1,6], Yared Hailemichael[1], Willem W. Overwijk[1,2], Navin Varadarajan[3], Roza Nurieva[2,7], Laszlo G. Radvanyi[1], Patrick Hwu[1,2], and Chantale Bernatchez[1,2]

Abstract

Purpose: Adoptive T-cell therapy using autologous tumor-infiltrating lymphocytes (TIL) has shown an overall clinical response rate 40%–50% in metastatic melanoma patients. BTLA (B-and-T lymphocyte associated) expression on transferred CD8$^+$ TILs was associated with better clinical outcome. The suppressive function of the ITIM and ITSM motifs of BTLA is well described. Here, we sought to determine the functional characteristics of the CD8$^+$BTLA$^+$TIL subset and define the contribution of the Grb2 motif of BTLA in T-cell costimulation.

Experimental Design: We determined the functional role and downstream signal of BTLA in both human CD8$^+$ TILs and mouse CD8$^+$ T cells. Functional assays were used including single-cell analysis, reverse-phase protein array (RPPA), antigen-specific vaccination models with adoptively transferred TCR-transgenic T cells as well as patient-derived xenograft (PDX) model using immunodeficient NOD-scid IL2Rgammanull (NSG) tumor-bearing mice treated with autologous TILs.

Results: CD8$^+$BTLA$^-$ TILs could not control tumor growth *in vivo* as well as their BTLA$^+$ counterpart and antigen-specific CD8$^+$BTLA$^-$ T cells had impaired recall response to a vaccine. However, CD8$^+$BTLA$^+$ TILs displayed improved survival following the killing of a tumor target and heightened "serial killing" capacity. Using mutants of BTLA signaling motifs, we uncovered a costimulatory function mediated by Grb2 through enhancing the secretion of IL-2 and the activation of Src after TCR stimulation.

Conclusions: Our data portrays BTLA as a molecule with the singular ability to provide both costimulatory and coinhibitory signals to activated CD8$^+$ T cells, resulting in extended survival, improved tumor control, and the development of a functional recall response. *Clin Cancer Res; 23(20); 6151–64. ©2017 AACR.*

Introduction

Adoptive T-cell therapy (ACT) using the body's own expanded tumor-infiltrating lymphocytes (TIL) with prior lymphodepletion and followed by high-dose IL-2 administration has demonstrated an overall response rate of 38%–51% in multiple clinical trials for stage IIIC/IV metastatic melanoma (1–4). A comprehensive immunophenotyping of TIL infusion products has revealed an unexpected finding that a population of CD8$^+$ TILs expressing a molecule known to attenuate T-cell response, the B and T lymphocyte associated (BTLA), was strongly associated with a positive clinical response (4).

BTLA is an inhibitory molecule expressed by T cells, B cells, dendritic cells, and NK cells (5). Herpes virus entry mediator (HVEM), a TNF receptor superfamily member 14 (TNFRSF14), is the known ligand for BTLA (6). The cytoplasmic domain of BTLA consists of three motifs; an immunoreceptor tyrosine-based inhibition motif (ITIM), an immunoreceptor tyrosine-based switch motif (ITSM), and a growth factor receptor–bound protein 2 motif (Grb2). Ligation of BTLA by HVEM has been shown to recruit Src homology 2 (SH2) domain-containing phosphatase 1 and 2 (SHP-1 and SHP-2) to the ITIM and ITSM motifs, resulting in suppression of T-cell receptor (TCR) activation (5, 7). Indeed, ITIM and ITSM motifs were required for the full function of BTLA to inhibit T-cell proliferation and cytokine production including IFNγ, IL-2, and IL-10 (8, 9). A recent report indicated that PD-1 ligation, which also contains ITIM and ITSM motifs, selectively inhibits both the Akt and Ras–MEK–ERK pathways (10). So far, it remains inconclusive whether BTLA utilizes mechanism similar to PD-1 as ITIM and ITSM motifs are commonly shared between these two receptors.

Unlike PD-1, BTLA also harbors a Grb2 motif. Although the function of the Grb2 motif remains unclear, some evidence suggests that it may actually transmit a positive signal. In fact, an *in vitro* binding assay demonstrated the potential interaction of

[1]Department of Melanoma Medical Oncology, The University of Texas MD Anderson Cancer Center, Houston, Texas. [2]Graduate Program in Immunology, Graduate School of Biomedical Sciences, The University of Texas Health Science Center at Houston, Houston, Texas. [3]Department of Chemical and Biomolecular Engineering, Cullen College of Engineering, University of Houston, Texas. [4]Graduate Program in Biostatistics, School of Public Health, The University of Texas Health Science Center at Houston, Houston, Texas. [5]Immunology Platform, Department of Immunology, The University of Texas MD Anderson Cancer Center, Houston, Texas. [6]Department of Genomic Medicine, The University of Texas M.D. Anderson Cancer Center, Houston, Texas. [7]Department of Immunology, The University of Texas MD Anderson Cancer Center, Houston, Texas.

Note: Supplementary data for this article are available at Clinical Cancer Research Online (http://clincancerres.aacrjournals.org/).

Current address for L.G. Radvanyi: Global Immuno-Oncology Research, EMD Serono Research Institute, Billerica, Massachusetts.

Corresponding Author: Chantale Bernatchez, The University of Texas M.D. Anderson Cancer Center, 7455 Fannin St., Houston, TX 77054. Phone: 713-563-8830; Fax: 713-745-0134; E-mail: cbernatchez@mdanderson.org

doi: 10.1158/1078-0432.CCR-16-1217

©2017 American Association for Cancer Research.

Downloaded from clincancerres.aacrjournals.org on October 21, 2020. © 2017 American Association for Cancer Research.

Published OnlineFirst July 28, 2017; DOI: 10.1158/1078-0432.CCR-16-1217

Translational Relevance

BTLA (B-and-T lymphocyte associated) is a negative T-cell cosignaling molecule. Its expression on $CD8^+$ tumor-infiltrating lymphocytes (TIL) unexpectedly associated with better clinical outcome in metastatic melanoma patients treated with adoptive T-cell therapy using TILs. We sought to determine whether BTLA signaling could positively impact T cells. Our results demonstrate that the $CD8^+BTLA^+$ TIL subset has a survival advantage following the killing of a tumor target in comparison with its $BTLA^-$ counterpart, which may explain the superior *in vivo* persistence of this subset after TIL infusion. Interestingly, the Grb2 motif of BTLA was found to promote IL-2 production following BTLA engagement in the context of a TCR stimulation, and the presence of BTLA on $CD8^+$ T cells was required to develop a robust recall response. Therefore, developing a strategy to selectively expand and infuse $CD8^+BTLA^+$ TILs may enhance TIL persistence postinfusion and result in superior clinical outcome.

the Grb2-binding motif with the Grb2 adaptor protein and the p85 subunit of phosphatidylinositol 3-kinase (p85 PI3K; refs. 7, 11). Interestingly, a gene expression analysis of mouse $CD4^+$ T cells following activation by anti-CD3 and anti-BTLA demonstrated a highly overlapping transcription profile with that produced by anti-CD3 in combination with positive costimulators (CD28, ICOS, and CD80), but not with inhibitory molecules (PD-1 and CTLA-4; ref. 12).

Emerging evidence also demonstrates that BTLA serves as a T-cell differentiation marker in human T cells as BTLA expression is highly enriched in naïve T cells and central memory T cells (Tcm) and downregulated upon T-cell differentiation (13). Our recent work demonstrated that $CD8^+BTLA^+$TILs exhibited the molecular signature of less-differentiated T cells as compared with their $CD8^+BTLA^-$ counterpart and had increased persistence following adoptive transfer in treated patients (14). Several studies in both immunodeficient murine and non-human primate models also demonstrated that central memory–derived effector $CD8^+$ T cells established a pool of *in vivo* persistent memory T cells (15–18). In addition, adoptive transfer of memory T cells with stem cell properties (T_{SCM}) was shown to confer *in vivo* persistence and better tumor control due to enhanced survival and antitumor properties (15).

Thus far, it remains understudied whether the intrinsic properties of less-differentiated TILs highly enriched in BTLA-expressing cells and/or BTLA signaling itself contribute to the favorable clinical outcome of TIL-treated patients. In this study, we have uncovered survival advantages of the $BTLA^+$ subset that allows for serial killing of target tumor cells, which may explain our previous correlation between this subset and response to TIL ACT. In addition, our results unveiled a role for the BTLA-associated Grb2-binding motif in T-cell proliferation and IL-2 production following TCR engagement that was independent of the inhibitory function of ITIM/ITSM motifs. The use of a pmel BTLA knockout system demonstrates a weaker priming of T cells in response to the cognate antigen and the absence of a recall response. Overall, this study has uncovered a previously unappreciated role of the Grb2 motif of BTLA in providing positive costimulatory signal to T cells and the ability of $CD8^+BTLA^+$TIL to function as serial killers.

Materials and Methods

Cell lines

Platinum-E retroviral packaging cell line, MEL 526 tumor line, and primary melanoma tumor cell line #2549, as well as B16F10, and B16OVA were maintained in Roswell Park Memorial Institute (RPMI) medium supplemented with 10% FBS (Gemini bio product), 10 mmol/L HEPES (Gibco), 10 mmol/L penicillin–streptomycin (Gibco), and 10 mmol/L Glutamine (Gibco), selenium–transferrin–insulin (Gibco), and 0.05 mmol/L β-mercaptoethanol (Gibco) as described previously (2, 19). Platinum-E retro packing cell line was purchased from Cell Biolabs. MEL 526 tumor line was obtained from Dr. Steven A. Rosenberg at the National Cancer Institute. Autologous primary melanoma tumor cell line #2549 was generated at MD Anderson Cancer Center (Houston, TX) from a tumor sample of a patient enrolled on an ongoing adoptive T-cell therapy study. The cell line #2549 was last authenticated on 03/24/2015 by STR DNA fingerprinting using the Promega 16 High Sensitivity STR Kit (Catalog #DC2100). The STR profiles were compared to online search databases (DSMZ/ATCC/JCRB/RIKEN) of 2,455 known profiles; along with the MD Anderson Characterized Cell Line Core (CCLC) database of 2,556 known profiles. The STR profiles matched known DNA fingerprint of patient's PBMCs. No authentication was performed in all other cell lines.

Patient tumor sample acquisition

Tumor samples were obtained from patients with stage IIIc and stage IV melanoma undergoing surgery at The University of Texas MD Anderson Cancer Center according to an Institutional Review Board–approved protocol and with patient consent (IRB# 2004-0069, LAB06-0755, NCT00338377). This study was carried out in compliance with the protocol and Good Clinical Practice concerning medical research in humans, as described in the Declaration of Helsinki.

Generation of TILs

Fragments from melanoma tumors were cut into 1 to 2 mm^3. Each fragment was placed into a single wells in 24-well culture plates (Falcon) and maintained with RPMI supplemented with 10% heat-inactivated Human AB serum (Gemini bio product), IL-2 6,000 IU/mL (Proleukin, Novartis), 10 mmol/L HEPES, 10 mmol/L penicillin–streptomycin (Gibco), and 10 mmol/L Glutamine (Gibco) as described previously (20).

Retroviral constructs of BTLA wild-type and mutants

Murine BTLA was amplified from fully sequenced murine BTLA from Mammalian Gene Collection Clones (MGC, Open Biosystems) by PCR with primers mBTLA-F and R (Supplementary Table S1). The PCR products were cloned into pRVKM retroviral vectors. To generate BTLA mutants, we substituted tyrosine for phenyl alanine in either Grb2 motifs or ITIM and ITSM motifs of BTLA cytoplasmic tails (Supplementary Table S2). These included murine ΔGrb2 mutants (Y245F), and murine Δ ITIM and ITSM mutants (Y274F and Y299F). Sequences of all constructs were validated by DNA sequencing.

Retroviral transduction of mouse BTLA-KO-T cells

pRVKM retroviral vectors and pEco plasmids were cotransfected into Plate-E cells using using PolyJet (Signagen Laboratories). The supernatants were harvested 60 hours later and

Downloaded from clincancerres.aacrjournals.org on October 21, 2020. © 2017 American Association for Cancer Research.

Published OnlineFirst July 28, 2017; DOI: 10.1158/1078-0432.CCR-16-1217

concentrated using Vivaspin-20 (Vivaproducts). Splenocytes from OT-1 BTLA KO mice were cultured with RPMI1640 with 10% FBS and hIL-2 at 300 IU/mL, and activated with anti-mouse CD3 at a concentration of 0.3 μg/mL (Clone 145-2C11, eBioscience) for 24 hours. The cells were then infected with a concentrated retrovirus and further expanded in RPMI1640 with 10% FBS and hIL-2 for 3 days. The cells were sorted on the basis of the expression of GFP using a FACSAria (BD Biosciences) and propagated with hIL-2 at 300 IU/mL for 5 days.

Reverse-phase protein array

Murine OT-1 BTLA KO cells overexpressing BTLA WT or mutants constructs were restimulated with either 10 ng/mL anti-mouse CD3 (Clone 145-2C11, BD Pharmingen) alone or with recombinant mouse HVEM Fc (R&D Systems) plate-bound for 8 hours prior to harvest with the cell lysis buffer (kindly provided by RPPA core facility at The University of Texas MD Anderson Cancer Center). The cell lysates were centrifuged at 14,000 rpm for 10 minutes at 4°C. The protein supernatant was quantified using protein assay kit (Thermo Scientific). Reverse-phase protein array (RPPA) was processed and normalized as described previously (21). Differential fold expression of protein was analyzed using Linear models and empirical Bayes methods (22). Volcano plots were generated using R system. For human TILs, four TIL lines were stained with anti-CD8 (clone RPA-T8, BD Pharmingen), anti-BTLA (clone J168, BD Pharmingen), and Sytox blue (Molecular Probe) under aseptic condition. The cells were sorted on the basis of expression of CD8$^+$BTLA$^+$ using FACSAria (BD Biosciences). On the next day, sorted TILs were restimulated with anti-human CD3 (clone OKT-3, eBioscience) with or without recombinant human HVEM-Fc (R&D Systems) plate-bound for 8 hours prior to harvest with the cell lysis buffer. The protein samples were processed, normalized, and analyzed as similar to the mouse experiment described above.

Intracellular cytokine staining

OT-1 BTLA KO T cells overexpressing BTLA WT or mutants were re-activated with either dendritic cells pulsed with OVA peptide (SIINFEKL; American peptide) or dendritic cells alone at ratio of 1:40 in the presence of BD GolgiStop (according to the manufacturer's instructions; BD Pharmingen). After 4 hours, the cells were fixed and permeabilized using BD Cytofix/Cytoperm kits (according to the manufacturer's instructions; BD Pharmingen), and subsequently stained with anti-mouse IFNγ (clone XMG1.2; BD Pharmingen) and anti-mouse TNFα (clone MP6-XT22; BD Pharmingen).

Cytokine multiplex assays

Murine OT-1 BTLA KO cells overexpressing BTLA WT or mutants were restimulated with either 10 ng/mL anti-mouse CD3 (Clone 145-2C11, BD Pharmingen) alone or with recombinant mouse HVEM-Fc (R&D Systems) plate-bound for 24 hours. Supernatants were collected to quantify the secreted cytokines using a MILLIPLEX MAP Mouse CD8$^+$ T Cell Magnetic Bead Panel (Millipore).

Killing assays

T cells were cocultured with tumor cells labeled with eFluor670 at ratio of 1:1, 1:3, and 1:10. After 3 hours, the cells were fixed and permeabilized using BD Cytofix/Cytoperm (according to manufacturer's protocol; BD Pharmingen), then stained with anti-cleaved caspase-3 (clone CPP32; BD Pharmingen), and analyzed by a BD FACSCanto II (BD Biosciences).

Cell proliferation assay

Murine OT-1 BTLA KO expressing BTLA WT or mutants were labeled with eFluor670 and restimulated with dendritic cells alone or dendritic cells pulsed with OVA peptide (SIINFEKL; American peptide) at a ratio of 1:40 for 48 hours prior to being analyzed using a BD FACSCanto II (BD Biosciences).

Nanowell array–based cytolytic assay

TILs and tumor cells were labeled with 1 μmol/L of red fluorescence dye (PKH26, Sigma) and 1 μL of green fluorescence dye (PKH68, Sigma), respectively. The cells were loaded onto nanowells at concentration of 1×10^6/mL. Target cell cytolysis mediated by TILs was monitored using a Carl Zeiss Axio Observer fitted with Hamamatsu EM-CCD camera using 10 × 0.3 NA objective. Apoptotic cells became green when stained with Annexin V conjugated with Alexa 647 as described previously (23).

In vivo killing of melanoma tumors using an NSG ACT model

NOD-*scid* IL2Rgamma^{null} (NSG) mice were engrafted with either 5×10^6 MEL 526 MEL tumor cells or 5×10^6 autologous primary melanoma tumor cells. On day 12, either 1×10^7 sorted CD8$^+$BTLA$^+$ or sorted CD8$^+$BTLA$^-$ were adoptively transferred into tumor-bearing mice (n = 5–8 per group). Recombinant human IL-2 (Proleukin, Prometheus) was administered intraperitoneally at a concentration of 6×10^5 IU immediately after the TIL transfer and daily for three days. Tumor size was measured every other day. Mice were sacrificed when tumors exceeded 15 mm diameter. Peripheral blood was collected every other day, lysed with ACK lysis buffer, then stained for AQUA (Invitrogen), anti-human CD45 (clone HI30; BD Pharmingen), and anti-human CD8 (clone RPA-T8; BD Pharmingen).

Vaccination model

C57BL/6J mice were intravenously administered 0.5×10^6 naïve pmel-1 or OT-I T cells, and vaccinated with gp100 peptide or OVA peptide (100 μg) together with anti-CD40 (50 μg) and imiquimod (50 mg). Recombinant human IL-2 at 1.2×10^6 IU was administered once, and 6×10^5 IU twice daily for the next 2 days (i.p.). Peripheral blood was collected every other day to determine the frequency of circulating pmel or OT-I T cells. Mice were boosted with gp100 or OVA peptide following the contraction phase and peripheral blood was collected every other day. Mice were sacrificed on day 120, and splenocytes were isolated to determine the presence of pmel T cells.

Animals

NOD-*scid* IL2Rgamma^{null} (NSG) mice were purchased from the Jackson Laboratory. OT-1 BTLA KO C57BL/6 and Pmel BTLA KO C57BL/6 mice were kindly provided from Dr. Roza Nurieva (Department of Immunology, The University of Texas MD Anderson Cancer Center, Houston, Texas and Graduate Program in Immunology, Graduate School of Biomedical Sciences, The University of Texas Health Sciences Center at Houston, Houston, Texas). Pmel BTLA WT C57BL/6 mice were kindly provided by Dr. Willem Overwijk (Department of Melanoma Medical Oncology, The University of Texas MD Anderson Cancer Center, Houston, Texas and Graduate Program in Immunology, Graduate

Downloaded from clincancerres.aacrjournals.org on October 21, 2020. © 2017 American Association for Cancer Research.

Published OnlineFirst July 28, 2017; DOI: 10.1158/1078-0432.CCR-16-1217

School of Biomedical Sciences, The University of Texas Health Sciences Center at Houston, Houston, Texas). C57BL/6 mice were purchased from Charles River Laboratories. All mice were housed in a specific pathogen-free facility at The University of Texas MD Anderson Cancer Center. Animal protocols were approved by The University of Texas MD Anderson Cancer Center [#00001229 (RN)].

Statistical analyses

Statistical analyses were performed using GraphPad Prism and the R system. For all survival curve analysis data, a log-rank test was used to compare distribution of the two groups. We applied Linear models and empirical Bayes methods to compare the differential protein expression from RPPA datasets. Differences in tumor cell death of B16-OVA and B16-F10 and the percentages of positive virally transduced mouse T cells producing IFNγ and TNFα were analyzed using a two-way ANOVA, and a two-tailed Student *t* test was used to determine statistical significance for all other analyses.

Results

High expression of CD8a and BTLA correlates with an improved survival of stage III metastatic melanoma patients

To investigate whether BTLA is associated with melanoma patient survival, we conducted a Kaplan–Meier survival analysis in stage III metastatic melanomas according to gene expression data in tumor tissues from TCGA (The Cancer Genome Atlas; ref. 24). We found that patients expressing high transcript levels of either CD8a or BTLA had much better survival as compared with either CD8a low or BTLA low, respectively (CD8a high vs. CD8a low, $P = 0.0007$, $N = 42$; BTLA high vs. BTLA low, $P = 0.001$, $N = 42$; Fig. 1A and B). When both markers were analyzed together, the association of CD8a high and BTLA high conferred the greatest survival benefit as compared with other combinations (CD8a high BTLA high vs. CD8a low BTLA low, $P = 0.0006$, $N = 98$) (Fig. 1C). BTLA can be expressed by immune cells other than T cells such as NK cells, B cells, or dendritic cells, with the highest levels found in B cells (5). Interestingly, we did not observe improved survival in patients with high BTLA expression when associated with either high NK cells (identified by the expression of NCR1) or B cells (CD19; Supplementary Fig. S1A and S1B). These data suggest that high BTLA expression in association with high $CD8^+$ signal is associated with improved melanoma patient survival. The coexpression of CD8 and BTLA cannot be inferred by gene expression profiling from tumor tissue; however, the improved survival benefit measured in conjunction with BTLA and CD8 expression is not seen when BTLA is evaluated in conjunction with markers from other cell populations known to express BTLA. These data lend support to our hypothesis that $CD8^+BTLA^+$ TILs exert efficient antitumor control based on our previous observation that this T-cell population correlated with better response to TIL ACT (4).

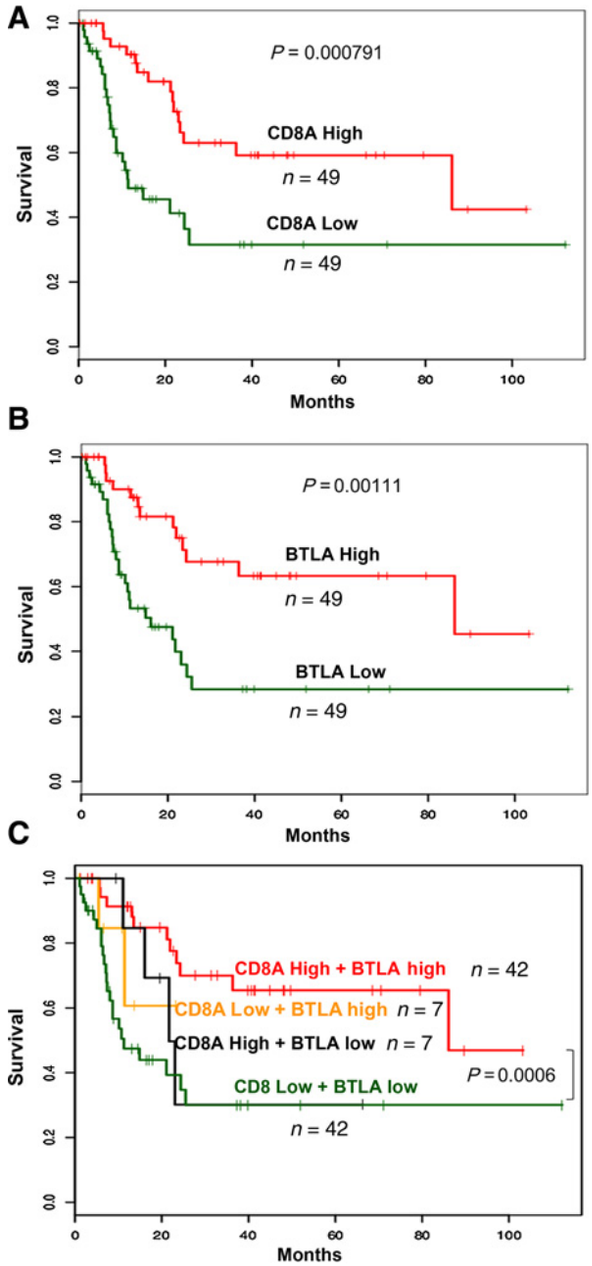

Figure 1.

Correlation of BTLA and CD8a coexpression with overall survival in stage III melanoma. Kaplan–Meier survival curves in stage III metastatic melanoma from The Cancer Genome Atlas (TCGA) consortium depicts: (**A**) CD8a expression; CD8a high versus CD8a low (**B**) BTLA expression; BTLA high versus BTLA low (**C**) Combined CD8 and BTLA expression; CD8a high BTLA high versus CD8a low BTLA high versus CD8a high BTLA low versus CD8a low BTLA low. Total number of patients = 98, (high- above median, low-below median). Statistical significance was determined using a log-rank. ($P < 0.001$ and $P < 0.0001$).

$CD8^+BTLA^+$TIL subset exhibits greater *in vivo* tumor control

It has been noted that more differentiated T cells secrete more cytotoxic and cytolytic proteins compared with less-differentiated T cells (25). Thus, we conducted both *in vitro* and *in vivo* tumor control studies to compare the killing capacity of the $BTLA^+$ and $BTLA^-$ $CD8^+$ TIL subsets. To determine CTL-mediated tumor killing and ensure an equal tumor-specific population of both BTLA subsets, MEL 526 melanoma tumor cells expressing the MART-1 antigen were cocultured with either sorted MART-1 recognizing (tetramer positive) $CD8^+BTLA^+$ ($CD8^+$MART-1^+BTLA^+) or $CD8^+BTLA^-$ ($CD8^+$MART-1^+BTLA^-). We found

Downloaded from clincancerres.aacrjournals.org on October 21, 2020. © 2017 American Association for Cancer Research.

Published OnlineFirst July 28, 2017; DOI: 10.1158/1078-0432.CCR-16-1217

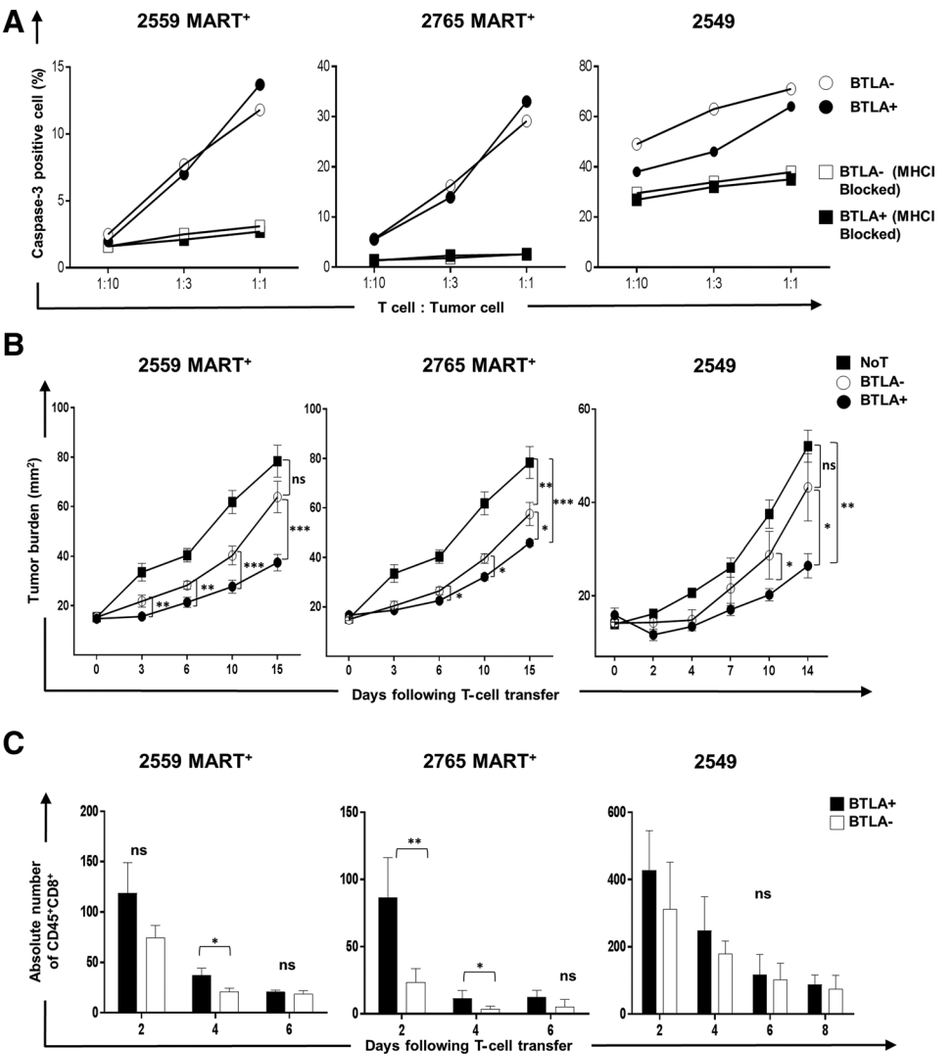

Figure 2.

CD8$^+$BTLA$^+$ TIL demonstrate a superior antitumor effect *in vivo*. **A,** MART1-reactive CD8$^+$ TIL (left and middle) and TIL 2549 (right) were sorted into BTLA$^+$ and BTLA$^-$ subsets. MEL 526 (melanoma tumor expressing MART-1 antigen, left and mid graph) or autologous tumor line 2549 (right graph) were stained with eFluor670 and cocultured with TILs at the following TIL-to-tumor cell ratios (1:10, 1:3, and 1:1). Tumor cell death is measured by the percentage of caspase-3–positive cells. **B,** Ten million sorted CD8$^+$BTLA$^+$ or sorted CD8$^+$BTLA$^-$ TILs were intravenously injected into tumor bearing mice previously subcutaneously implanted with either MEL 526 or autologous melanoma tumor line 2549. Tumor burden was measured using calipers and diameter graphed as mm^2. **C,** Bar graph shows the percentage of CD45$^+$CD8$^+$ in the peripheral blood on days 2, 4, 6, and 8 post-adoptive transfer in the same experiment described in **B**. $N = 5$–8 animals per group. *, $P < 0.05$; **, $P < 0.001$; ***, $P < 0.0001$. All values in figure are expressed as mean ± SEM. *P* values were calculated using a two-tailed Student *t* test.

comparable MART-1 antigen-specific tumor killing ability after a short term (3 hours) TIL and tumor coincubation between the BTLA$^+$TIL and BTLA$^-$TIL subsets in two TIL lines (Fig. 2A, left TIL#2559; middle, TIL #2765). In addition, comparable killing ability was observed using bulk nonantigen-restricted, sorted BTLA subsets in a third TIL line (Fig. 2A, right, TIL #2549). As we did not observe a difference in *in vitro* killing between the two subsets, but have demonstrated a better clinical outcome in patients infused with more CD8$^+$BTLA$^+$ TILs, we next determined whether this subset could exhibit better *in vivo* tumor control. Immunodeficient NOD-*scid* IL2Rgamma^{null} mice (NSG) were engrafted with 5×10^6 MEL 526 human melanoma tumor cells for 10 days prior to adoptive transfer of 1×10^7 human CD8$^+$MART$^+$BTLA$^+$TILs or CD8$^+$ MART$^+$BTLA$^-$TILs. Tumor burden was measured every other day and transferred TILs were quantified from peripheral blood based on the expression of CD45 and CD8. We observed that the CD8$^+$BTLA$^+$ TIL subset exhibited significantly better tumor control on day 14 as compared with its BTLA$^-$ counterpart in NSG mice treated with either MART-1 tumor antigen–restricted TIL line [2559 MART$^+$; $P = 0.002$ (Fig. 2B, left) and 2765 MART$^+$; $P = 0.042$ (Fig. 2B, middle)] as well as in a nontumor antigen–restricted setting (2549; $P = 0.049$; Fig. 2B, right). In addition, we found that the level of the CD8$^+$BTLA$^+$ TIL subset in the peripheral blood was significantly higher than the CD8$^+$BTLA$^-$ subset early after therapy in mice treated with antigen-specific TIL lines [2559 MART$^+$; $P = 0.039$ on day 4, (Fig. 2C, left) 2765 MART$^+$; $P = 0.0021$ and 0.02 on day 2 and 4, respectively (Fig. 2C, middle)], but not in those treated with the nonrestricted antigen-specific TIL line (2549; $P = 0.06$ on day 2; Fig. 2C, right). In summary, these data suggests that the CD8$^+$BTLA$^+$ and CD8$^+$BTLA$^-$ TIL subsets are equally able to directly kill tumor targets in a short-term *in vitro* assay. However, the BTLA-positive subset provides superior *in vivo* tumor control and tends to persist better following TIL transfer.

Shorter target seeking but longer target killing time for CD8$^+$BTLA$^+$ TIL subset

As demonstrated above, the CD8$^+$BTLA$^+$ subset provides significantly better tumor control than its CD8$^+$BTLA$^-$ counterpart *in vivo;* however, this difference is not observed in an *in vitro* setting. Because our previous *in vitro* tumor killing experiments were conducted using population assays and for only 3 hours, this

Downloaded from clincancerres.aacrjournals.org on October 21, 2020. © 2017 American Association for Cancer Research.

Published OnlineFirst July 28, 2017; DOI: 10.1158/1078-0432.CCR-16-1217

limited our ability to track T-cell fate following tumor target cell interactions. To further understand the behavioral difference between the $CD8^+BTLA^+$ and $CD8^+BTLA^-$ subsets in mediating tumor killing, we utilized Timelapse Imaging Microscopy In Nanowell Grids (TIMING), to study the dynamic interactions between individual tumor targets and effector T cells in high-throughput (26, 27). To this end, labeled tumor cells and TILs were loaded onto the nanowell chip, consisting of 28,224 wells regularly separated in 7 × 7 blocks, and the interactions were quantified at two separate effector-to-target cell ratios of 1:1 and 1:2. This assay allowed us to dissect the kinetics of T-cell killing by calculating the following sequential parameters: (i) Time needed to establish conjugation between the T cell and tumor target (t_{seek}), (ii) duration of the contact between the T cell and the tumor target ($t_{contact}$), and (iii) time between the first T-cell contact with the tumor cell and tumor cell apoptosis (t_{death}; Fig. 3A). Interestingly, the $CD8^+BTLA^+$ subset was more efficient in tumor seeking at effector-to-target cell ratios of 1:1 ($N = 3{,}319$) as the time utilized to make first contact with tumor cells was significantly less than that of the $CD8^+BTLA^-$ subset ($P < 0.0001$; Fig. 3B, left). This difference was not observed when 2 targets were present in the well (1:2, $P = 0.22$) (Fig. 3B, left). It is possible that loading 2 targets in each nanowell rendered the distance to travel to meet each target too short to be able to measure a difference in the ability of T-cell subsets to seek the target. However, in comparison with $CD8^+BTLA^-$ TILs, individual $CD8^+BTLA^+$ TILs spent longer time in contact with a tumor cell target and induced apoptosis with slower kinetics at both E:T ratios studied ($t_{contact}$; 1:1 and 1:2, $P < 0.0001$, t_{death}; 1:1 and 1:2, $P < 0.0001$; Fig. 3B, middle and right, respectively). Overall, individual $CD8^+BTLA^+$ TILs found their target faster, but required longer durations to complete tumor cell killing (Supplementary Movie S1 and S2).

$CD8^+BTLA^+$ TIL subset is characterized by a heightened ability to kill multiple targets

We next examined whether one subset was more potent in its overall tumor killing capacity by evaluating tumor target cell survival over the 8-hour coculture period. Overall, both T-cell subsets killed 18% of the tumor targets at an E:T ratio of 1:1 (Fig. 3C, red inner circle). However, at the 1:2 ratio, the $CD8^+BTLA^+$ subset was able to kill a total of 21% of the tumor targets upon contact as opposed to only 14% for the $CD8^+BTLA^-$ subset (Fig. 3C, red and green sections, outer circle). Second, when presented with two tumor targets, the $CD8^+BTLA^+$ subset was twice as likely to kill both targets (14% for the $BTLA^+$ vs. 7% for the BTLA; Fig. 3C).

Examination of the kinetics of tumor killing offered clues to understand the differences in the overall killing potential of the two subsets. The analysis of the full 500-minute assay revealed a different killing pattern early after tumor encounter (first 250 minutes) in comparison with the second half of the incubation (last 250 minutes). A close look at the first 250 minutes demonstrated that the $CD8^+BTLA^-$ subset was more effective in tumor killing than the $CD8^+BTLA^+$ subset as the survival of the contacted tumor targets dropped significantly faster when coincubated with $CD8^+BTLA^-$ TILs at effector-to-target cell ratios of 1:1 and 1:2 (left, 1:1, $P < 0.03$; right, 1:2, $P < 0.0001$; Fig. 3D). However, the overall percentage of killed targets at both ratios at the 250 minutes mark is the same between both TIL subsets. Therefore, the killing potential of the two subsets is comparable in the first 250 minutes but their kinetics of killing are different.

Over the last 250 minutes of the assay, the picture changes (Fig. 3E). The blue curve ($BTLA^+$) now dips below the red curve ($BTLA^-$), signifying that the $BTLA^+$ subset is catching up with the $BTLA^-$ subset in terms of the speed at which it kills (E:T ratio of 1:1, $P = 0.54$), or takes a significant lead (E:T ratio of 1:2, $P < 0.0001$). It is also worth noting that very limited killing occurs with the $BTLA^-$ in the second half of the experiment at any ratio while the $BTLA^+$ subset achieves higher killing when more targets are present in the well (1:2). We reasoned that this situation could be explained by a differential ability for serial killing, or the ability to kill a second target, which can only be detected if there is more than one target in the well therefore at a 1:2 ratio (Fig. 3E).

Improved survival of the $CD8^+BTLA^+$ TIL subset following killing of a target

After activation, T cells can be eliminated through the process of activation-induced cell death (AICD). The ability of the $CD8^+BTLA^+$ subset to kill multiple targets could be linked to an enhanced ability to survive AICD after completing its effector function. To test this hypothesis, we quantified effector T-cell death after a tumor killing event. We found that in fact, $CD8^+BTLA^-$ TILs are more susceptible to undergo apoptosis as compared with their $CD8^+BTLA^+$ TIL counterpart ($P < 0.01$; Fig. 3F). These data demonstrate that the $CD8^+BTLA^+$ subset survives better after killing a tumor target and thus is able to sustain its cytotoxic functionality and eliminate additional tumor cells. In summary, these results argue that both subsets kill equally well in a short-term killing assay (250 minutes) but the differences emerge when the T-cell and tumor coincubation is prolonged to 8 hours wherein the $CD8^+BTLA^+$ TIL subset is found to have an increased propensity to survive a killing event and therefore function as serial killers, thus confirming that the $CD8^+BTLA^+$ TIL subset is qualitatively better consistent with the *in vivo* results (Supplementary Movie S3).

Memory recall response is defective in BTLA-deficient T cells

Our data suggest a difference in survival of $BTLA^+$ antitumor $CD8^+$ T cells rather than a change in killing potential. We next sought to evaluate the long-term fate of $CD8^+BTLA^+$ antigen-specific T cells after *in vivo* antigenic challenge in an immunocompetent animal. Our study of the expression of BTLA in human and mouse $CD8^+$ T cells showed a different expression pattern (Supplementary Figs. S2 and S3). Murine naïve CD8 (CD44 low CD62L high) are negative for BTLA, but expression of BTLA is acquired as the cells differentiate to memory (CD44 high) while human naïve CD8 cells ($CCR7^+$, $CD45RA^+$) are positive for BTLA and expression is progressively lost as the CD8 cells differentiate to terminal effector cells (EMRA, $CCR7^-$, $CD45RA^+$). However, memory stages of differentiation are positive for BTLA in both mouse and human. On the basis of this, we reasoned that a vaccination model would be the most appropriate *in vivo* antigen trigger to measure the role of BTLA on the function of CD8. We aimed to measure the impact of BTLA expression on newly generated memory $CD8^+$ T cells on their capacity to respond to a second antigen exposure (recall). In this study, we sought to determine the role of BTLA in the persistence of antigen-specific $CD8^+$ T cells *in vivo* after antigenic stimulation. We used TCR transgenic $CD8^+$ T cells that are either WT or KO for BTLA and study their response to immunization and memory-recall

Downloaded from clincancerres.aacrjournals.org on October 21, 2020. © 2017 American Association for Cancer Research.

Published OnlineFirst July 28, 2017; DOI: 10.1158/1078-0432.CCR-16-1217

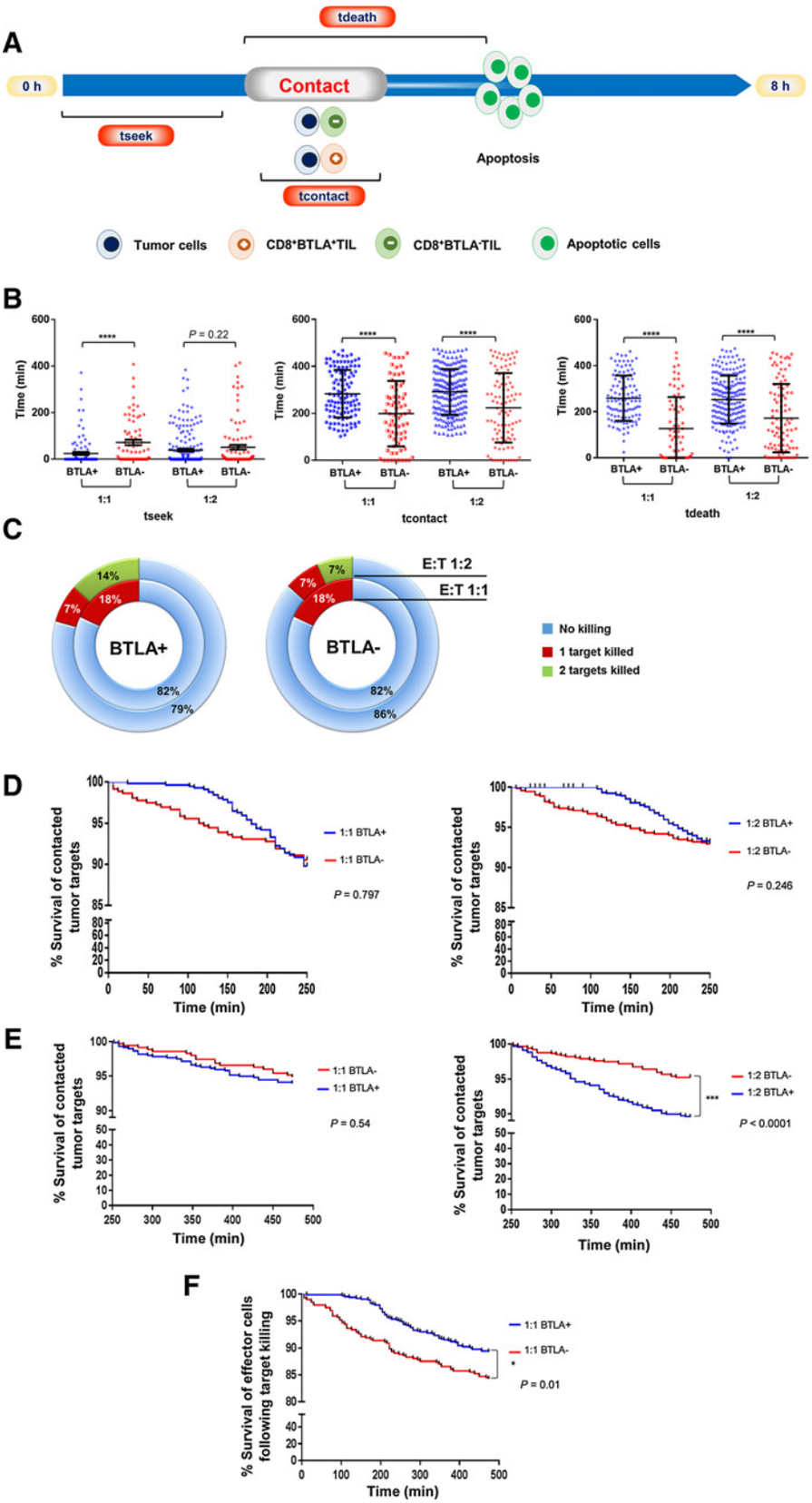

Figure 3.

CD8$^+$BTLA$^+$TIL subset mediates killing of multiple tumor targets through enhanced survival properties. Nanowell array–based cytolysis assay was used to determine tumor killing capacity at single-cell level. Effector cell and tumor target are labeled in different colors and loaded into the nanowell at effector-to-target cell ratios of 1:1 and 1:2. Interaction between effector and target cells is monitored by automated time-lapse camera coupled with a fluorescence microscope. **A,** Schematic diagram demonstrates the sequential events that effector cells seek (tseek), contact (tcontact), and mediate tumor cell death (tdeath). **B,** Either CD8$^+$MART$^+$BTLA$^+$ or CD8$^+$MART$^+$BTLA$^-$ subset was coincubated with MEL 526. Time (min) between each sequential event is evaluated. Dot plots depict tseek (left), tcontact (middle), tdeath (right) in comparison between CD8$^+$BTLA$^+$ (blue) and CD8$^+$BTLA$^-$ (red) subsets. All error bars depict the mean ± SEM. All *P* values were calculated using a two-tailed Student *t* test. ($N = 497$). **C,** Donut charts demonstrate the frequency of tumor cell death following effector cell killing by either CD8$^+$BTLA$^+$ (left)or CD8$^+$BTLA$^-$(right) subset. Inner circle and outer circle depict E:T ratio of 1:1 and 1:2, respectively. **D,** Kaplan–Meier survival curves of T-cell–contacted tumor target resulting in a killing event in the first 250 minutes in comparison between CD8$^+$BTLA$^+$ and CD8$^+$BTLA$^-$subsets at effector-to-target cells ratios of 1:1 (left) and 1:2 (right). **E,** Kaplan–Meier survival curves of T-cell–contacted tumor target resulting in a killing event in the last 250 minutes in comparison between CD8$^+$BTLA$^+$ and CD8$^+$BTLA$^-$subset at effector-to-target cells ratios of 1:1 (left) and 1:2 (right). Statistical significance in **D** and **E** was determined using a log-rank ($N = 3,319$; ***, $P < 0.0001$). **F,** Kaplan–Meier survival curves of tumor-contacted effector cells following tumor cell death in comparison between CD8$^+$BTLA$^+$ and CD8$^+$BTLA$^-$ subsets at an effector-to-target ratio of 1:1. Statistical significance was determined using a log-rank ($N = 3,319$; *, $P < 0.05$).

Downloaded from clincancerres.aacrjournals.org on October 21, 2020. © 2017 American Association for Cancer Research.

Published OnlineFirst July 28, 2017; DOI: 10.1158/1078-0432.CCR-16-1217

response using a mouse vaccination model as described previously (28). Splenocytes (5×10^5) from either Pmel-1 WT or Pmel-1 BTLA KO (recognizing gp100 peptide) were adoptively transferred into C57BL/6 recipient mice. On the following day, mice were vaccinated with gp100 peptide together with anti-mouse CD40. Imiquimod cream 5% was also applied on the vaccination site to boost the innate immune response. In addition, IL-2 was also provided to support *in vivo* T-cell proliferation following vaccination (Fig. 4A and B). The frequency of Pmel-1 T cells was tracked in peripheral blood after vaccination (Fig. 4C). On day 20 following priming, we observed a significantly higher frequency of Pmel-1 WT in peripheral blood when compared with Pmel-1 BTLA KO. The frequency of both Pmel-1 WT and Pmel-1 BTLA KO contracted to prepriming frequency by day 30. Boost vaccination was performed on day 60. We observed that Pmel-1 WT T cells had a robust recall response that was absent in the Pmel-1 BTLA KO group (Fig. 4C). To determine the impact on the generation of a long-term memory response, we assessed the frequency of Pmel-1 T cells in the spleen on day 120. We found a significantly higher percentage of Pmel-1 WT T cells in the spleen as compared with Pmel-1 BTLA KO T cells (Fig. 4D, $P = 0.038$). Similar data were obtained with the transfer of BTLA WT or KO OT-1 T cells and vaccination with OVA peptide SIINFEKL (Supplementary Fig. S4). In this context, the use of BTLA KO OT-1 T cells led to a marked attenuation of the recall response, but not the complete lack observed with the Pmel-1 T cells. Nonetheless, these results suggest that BTLA is critical for the generation of a recall memory response.

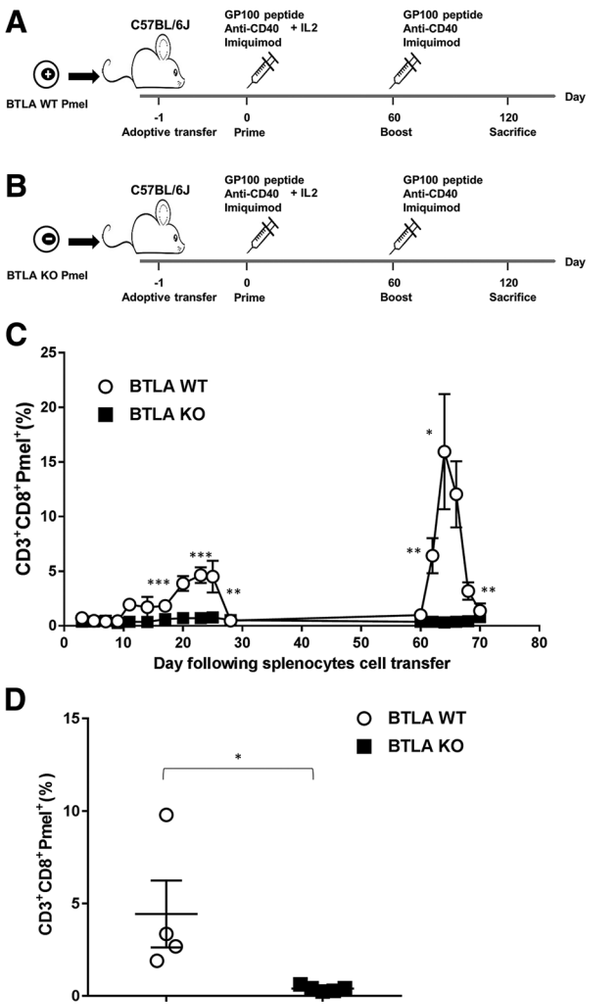

Figure 4.

Defective memory recall response of BTLA-deficient T cells. Schematic diagram depicting experimental design of mouse model for vaccination. 0.5×10^6 (**A**) Pmel-1 Thy 1.1. wild-type splenocytes or Pmel-1 BTLA KO splenocytes (**B**) were adoptively transferred into C57BL/6 mouse recipients (i.v.; $n = 5$ mice per group). On the following day, the recipients were vaccinated with gp100 peptide (100 μg) together with anti-CD40 (50 μg) and imiquimod (50 mg). Recombinant human IL-2 at 1.2×10^6 IU was administered once, and 6×10^5 IU twice daily for the next 2 days (i.p.). Peripheral blood was collected every other day to determine the frequency of circulating Pmel-1 Thy 1.1 T cells. On day 60, the mice were vaccinated with gp100 peptide, and peripheral blood was collected every other day until Pmel-1 T cells were no longer detected. On day 120, the mice were euthanized, and spleens were collected to determine the presence of Pmel-1 Thy 1.1 T cells. **C,** Plot graph depicts the percentage of $CD3^+CD8^+Pmel^+$ T cells in the peripheral blood following the priming (first peak from day 15 to day 30) and boosting (second peak from day 60 to 70). The frequency of $CD3^+CD8^+Pmel^+$T cells was significantly higher in C57BL/6 mouse recipients receiving Pmel-1 Thy 1.1 wild-type splenocytes as compared with those receiving Pmel-1 Thy 1.1 BTLA KO splenocytes. **D,** Comparison of the percentage of $CD3^+CD8^+Pmel^+$ T cell in spleen on day 120 of mice receiving either Pmel-1 Thy 1.1 wild-type splenocytes or Pmel-1 Thy 1.1 BTLA KO splenocytes. Pmel-1 Thy 1.1 BTLA KO splenocytes failed to develop memory recall response following vaccination and boosting.

Dichotomous BTLA signaling: ITIM/ITSM dampens effector cytokine secretion while Grb2 enhances IL-2 production

Our *in vivo* experiments with human TIL and single-cell killing analyses have suggested that the $CD8^+BTLA^+$ subset is endowed with a superior prosurvival function leading to better antitumor activity. Conceivably, the superiority of this subset could result from either (i) properties of less-differentiated T cells marked by BTLA expression or (ii) signaling through the BTLA molecule itself. Our vaccination study suggests a direct involvement of the BTLA molecule. However, to further test the contribution of the BTLA signaling, we performed functional studies of BTLA by overexpressing wild-type BTLA (WT BTLA) or variants of BTLA's intracellular motifs in OT-1 T cells from OT-1 BTLA KO mice. To dissect the signaling contributions from the ITIM/ITSM and the Grb2 motifs independently, retroviral constructs were generated with point mutations by substitution of tyrosine for phenylalanine in either the Grb2-binding motif (ΔGrb2) or the ITIM and ITSM motifs (ΔITSM; Fig. 5A). OT-1 BTLA KO T cells were transduced with constructs containing WT BTLA, ΔGrb2, and ΔITSM as well as an empty vector control (EM). Virally transduced OT-1 T cells were cocultured with either B16-F10 (negative for OVA antigen) or B16-OVA tumor cells at an effector-to-target ratio of 1:10, 1:3, and 1:1. HVEM expression on both tumor targets was confirmed by flow cytometry (Supplementary Fig. S5). Indeed, the tumor killing capacity of the TILs in this short-term *in vitro* assay was comparable regardless of the presence of WT BTLA or BTLA mutants at all ratios tested (ratio 1:1, $P = 0.67$; ratio 1:3, $P = 0.46$; ratio 1:10, $P = 0.29$; Fig. 5B). We did not observe differences in the number of T cells producing IFNγ or TNFα among these different groups (IFNγ, $P = 0.11$; TNFα, $P = 0.59$; Fig. 5C, left). However, the amount of effector cytokines being made by the WT BTLA-transduced T cells was significantly less than that made by those transduced with the empty vector alone following restimulation with dendritic cells pulsed with OVA peptide (IFNγ MFI; EM vs. WT, $P = 0.04$, TNFα MFI; EM vs. WT, $P = 0.0045$; Fig. 5C, right).

Downloaded from clincancerres.aacrjournals.org on October 21, 2020. © 2017 American Association for Cancer Research.

Published OnlineFirst July 28, 2017; DOI: 10.1158/1078-0432.CCR-16-1217

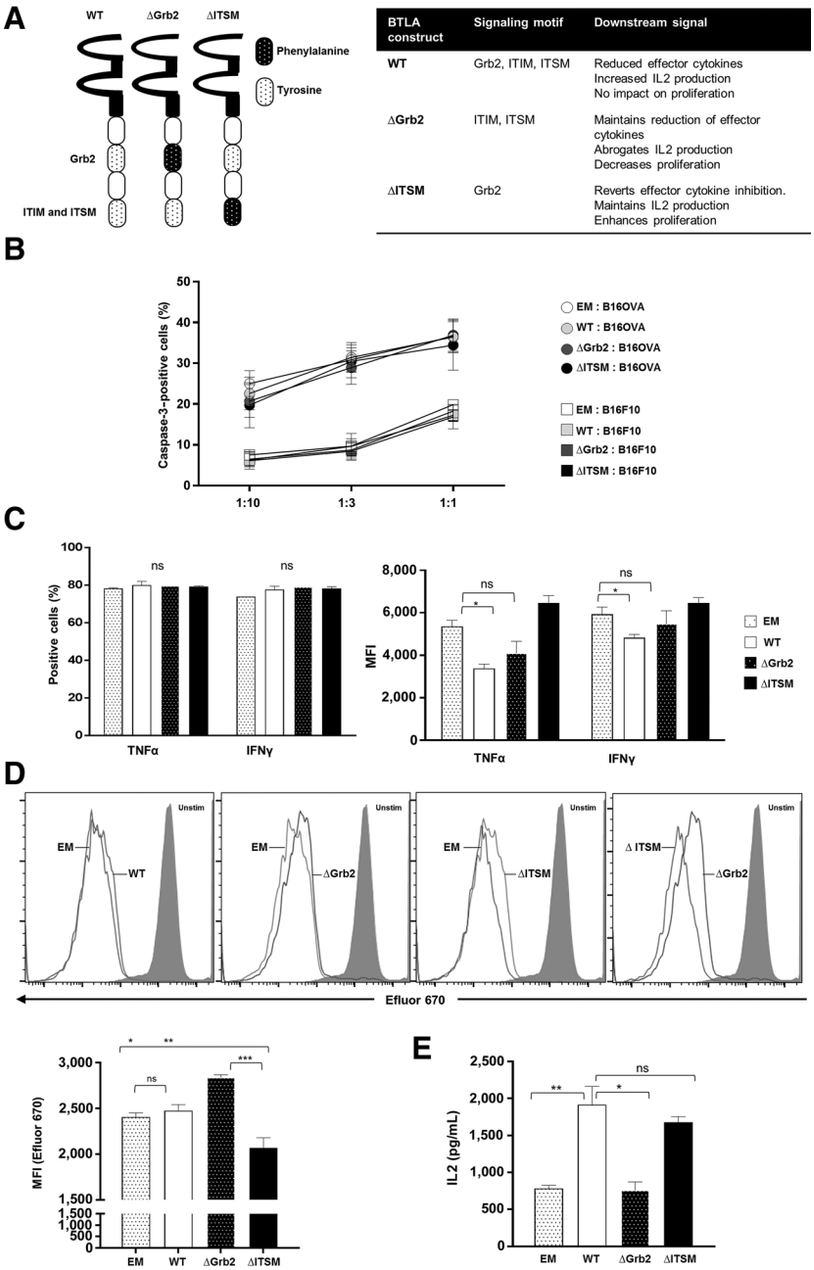

BTLA construct	Signaling motif	Downstream signal
WT	Grb2, ITIM, ITSM	Reduced effector cytokines Increased IL2 production No impact on proliferation
ΔGrb2	ITIM, ITSM	Maintains reduction of effector cytokines Abrogates IL2 production Decreases proliferation
ΔITSM	Grb2	Reverts effector cytokine inhibition. Maintains IL2 production Enhances proliferation

Figure 5.

BTLA signaling motifs show no effect on tumor killing, while Grb2 motif augments IL-2 production and T-cell proliferation. **A,** Schematic diagram depicts the structure of BTLA WT (left), BTLAΔGrb2 (middle), and BTLAΔITSM (right). Signaling motifs with modified Tyrosine to Phenylalanine are indicated by a dotted pattern over a black background. A table summarizing the phenotype observed with the expression of BTLA or of the different BTLA constructs is presented on the right. **B,** B16-OVA (mouse melanoma tumor positive for OVA) or B16-F10 (mouse melanoma tumor negative for OVA) were stained with eFluor670 and cocultured with OT-1 BTLA KO T cells overexpressing WT BTLA or BTLA mutants at the following T-cell-to-tumor cell ratios (1:10, 1:3, and 1:1). Tumor cell death is depicted by the percentage of caspase-3–positive cells. $N = 3$ independent experiments. **C,** OT-1 BTLA KO T cells overexpressing WT BTLA or its variants were restimulated with dendritic cells pulsed with OVA peptide. TNFα and IFNγ production by virally transduced OT-1 BTLA KO T cells was evaluated by intracellular staining. Bar graph depicts the percentage of positive cells (left) and mean fluorescence intensity (MFI; right). Each bar represents three independent experiments (two-way ANOVA; *, $P < 0.05$). **D,** OT-1 BTLA KO T cells overexpressing WT BTLA or its variants were labeled with eFluor670 and restimulated with dendritic cells pulsed with OVA peptide. Cell proliferation was determined by the dilution of eFluor670. Histogram plots of eFluor670 demonstrate proliferation of OT-1 BTLA KO T cells overexpressing WT BTLA or its variants. Bar graph depicts MFI of virally transduced T cells in the same experiment shown in the left. $N = 3$ *, $P < 0.05$; **, $P < 0.001$, ***, $P < 0.0001$. All error bars depict the mean ± SEM. All P values were calculated using a two-tailed Student t test. **E,** Virally transduced OT-1 BTLA KO T cells were stimulated with plate-bound anti-mouse CD3 and HVEM Fc. Supernatants were assessed for IL-2 production using MILLIPLEX MAP Mouse CD8$^+$ T Cell Magnetic Bead Panel Assays. Each bar graph represents two independent experiments. *, $P < 0.05$; **, $P < 0.001$. All error bars depict the mean ± SEM. All P values were calculated using a two-tailed Student t test.

Downloaded from clincancerres.aacrjournals.org on October 21, 2020. © 2017 American Association for Cancer Research.

Published OnlineFirst July 28, 2017; DOI: 10.1158/1078-0432.CCR-16-1217

The BTLA-mediated inhibition of IFNγ and TNFα production was relieved by the disruption of the ITIM/ITSM motifs; however, it was not significantly impacted by the disruption of the Grb2 motif, suggesting that ITIM and ITSM motifs are mainly involved in regulating the amount of effector cytokines produced following TCR triggering.

We have previously demonstrated that the $CD8^+BTLA^+$TIL subset had an improved proliferative capacity in response to IL-2 (14). Thus, we sought to determine whether BTLA signaling motifs could play a role in T-cell proliferation. OT-1 BTLA KO T cells overexpressing BTLA WT or mutants were labeled with the cell proliferation dye eFluor670 and restimulated with dendritic cells pulsed with OVA peptide for two days. T-cell proliferation was comparable between control and WT BTLA groups. (MFI: WT vs. EM; $P = 0.30$; Fig. 5D, histogram). On the other hand, subtle differences are appreciable between T cells expressing the different BTLA constructs. We observed that OT-1 BTLA KO T cells expressing ΔITSM had a lower mean fluorescence intensity (MFI) of the eFluor670 dye as compared with the empty vector control which is indicative of a more robust proliferation (MFI: ΔITSM vs. EM; $P = 0.012$, ΔITSM vs. WT; $P = 0.0057$; Fig. 5D). On the contrary, attenuation of T-cell proliferation was observed in T cells expressing a disrupted Grb2 motif (ΔGrb2), (MFI: ΔGrb2 vs. ΔITSM; $P = 0.0003$, ΔGrb2 vs. EM; $P = 0.0008$, ΔGrb2 vs. WT; $P = 0.0009$; Fig. 5D). These data suggest that the T-cell proliferation post TCR triggering is regulated positively by the Grb2 motif and negatively by ITIM/ITSM motifs.

Our previous report demonstrated that $CD8^+BTLA^+$ human TILs produce more IL-2 upon activation (14). Thus, we further investigated whether BTLA signaling could be responsible for IL-2 secretion. OT-1 BTLA KO T cells overexpressing WT BTLA or its mutants were restimulated with anti-CD3 in the presence of HVEM-Fc fusion protein to engage the BTLA molecule, and IL-2 secretion was assessed. Indeed, we found that IL-2 production was significantly increased in activated T cells transduced with the BTLA WT and ΔITSM constructs, but not in ΔGrb2 and the empty vector. This suggests that the BTLA-dependent IL-2 production was mediated through Grb2 motif, independently of the ITIM/ITSM motifs (WT vs. EM; $P = 0.02$, ΔITSM vs. EM; $P = 0.005$, WT vs. ΔGrb2; $P = 0.02$, ΔITSM vs. ΔGrb2; $P = 0.01$, EM vs. Grb2; $P = 0.79$, WT vs. ΔITSM; $P = 0.32$; Fig. 5E). These data highlight that Grb2 signaling contributes to IL-2 production following BTLA ligation during T-cell activation. A summary of the phenotypes seen with the expression of BTLA or its variants is presented in Fig. 5A (right).

Signaling downstream of mouse BTLA

To identify proteins activated downstream of BTLA, we employed RPPA, a high-throughput method developed for functional proteomic studies. OT-1 BTLA KO mouse T cells overexpressing WT BTLA or BTLA mutants were stimulated with anti-CD3 with or without HVEM-FC for 8 hours. The full list of tested proteins can be found in Supplementary Table S3. The protein expression levels found in activated T cells transduced with BTLA WT was used as a reference to compare the differential protein changes in ΔGrb2 and ΔITSM. The protein expression profile of the T cells expressing the BTLA variants were also compared with that obtained with the empty vector (Supplementary Table S4). We observed that the phosphorylation of Akt at T308 as well as the phosphorylation of one of its substrates, pPRAS40 at T246, were significantly attenuated in ΔGrb2 in comparison with BTLA WT (pAkt T308; $P = 0.045$, pPRAS40 T246; $P = 0.007$; Fig. 6A, left; Supplementary Table S4) (29). As expected, the disruption of ITIM/ITSM motif resulted in a remarkable enhancement of the phosphorylation of several proteins such as Src, Chk1, Chk2, as well as members of the Wnt pathway GSK-3b, and of β-Catenin at T41 and S45 (pSrc at S527; $P = 0.005$, pA-Raf at S299; $P = 0.01$, and pC-Raf at S338; $P = 0.02$, pChk1 at S286; $P = 0.01$, pChk2 at T68; $P = 0.02$, GSK-3b at S9; $P = 0.04$, β-Catenin at T41 and S45; $P = 0.04$; Fig. 6A, right; Supplementary Table S4).

BTLA-HVEM axis in human TILs selectively suppresses Akt and NFκB pathways but enhances Src pathway

To exclude the bias of overexpression of WT BTLA and genetically modified BTLA in BTLA knockout mouse, we further investigated BTLA signaling pathway in human TILs, which is more physiologically and clinically relevant to our observation in our adoptive T-cell therapy clinical trial. Sorted $CD8^+BTLA^+$ human TILs were stimulated with plate-bound anti-human CD3 at concentrations of 10, 30, 100, 300, and 1,000 ng/mL with or without HVEM-Fc for 8 hours and proteins extracted from cell lysates were used to perform RPPA in 5 separate patient TIL samples. We observed a general decrease in differentially phosphorylated protein changes in several signaling pathways when T-cell activation happened in the presence of HVEM. These included the MAPK kinase pathway (pP38 at T180; $P = 2.08 \times 10^{-9}$, pP90RSK at T573; $P = 3.26 \times 10^{-4}$, pS6 at S235; $P = 1.68 \times 10^{-2}$), NFκB pathway (pNFκB p65 at S536; $P = 3.15 \times 10^{-2}$), the Akt pathway (pAKT at S473; $P = 9.6 \times 10^{-3}$), and the β-catenin pathway (GSK-3a-b pS21; $P = 9.6 \times 10^{-3}$; Fig. 6B and C; Supplementary Table S5). Inhibition of these positive signaling pathways clearly supports the role of BTLA as a coinhibitory molecule. Interestingly, we found a significant elevation of Src phosphorylation at S416 (pSrc at S416; $P = 3.36 \times 10^{-6}$) when the T-cell activation happened in the presence of HVEM. Our results suggest that the TCR signaling pathway is not completely suppressed by BTLA, but is specifically attenuated in certain pathways as indicated above and specifically potentiated in very select pathway(s). Unexpectedly, we found that phosphorylation of HER2 at tyrosine 1248 was prominently increased in an anti-CD3 dose-dependent manner regardless of the presence of HVEM. This strengthens the notion that the BTLA/HVEM axis acts on specific targets. To further comprehensively understand the downstream signaling pathway of human BTLA, we generated the signaling network of proteins significantly changed during HVEM ligation using Ingenuity Pathway Analysis (IPA). We observed that Src signaling node was exclusively clustered and separated from Akt, NFκB, and β-catenin signaling nodes. This suggests that the Src signaling pathway is likely not or minimally interfered by SHP1/2 (Fig. 6D).

Discussion

Our recent report demonstrated that the $CD8^+BTLA^+$ TILs are less differentiated, respond better to IL-2, and persist longer in the patient postinfusion (14). In the current study, we shed light on the dichotomy of the signaling downstream of BTLA and highlight a role for BTLA in the development of $CD8^+$ T-cell memory-recall and the survival of effector memory $CD8^+$ T cells sustaining their antitumor function.

We observed that the $CD8^+$ $BTLA^+$ and $CD8^+$ $BTLA^-$ subsets had comparable *in vitro* killing, which did not explain the superiority of the $CD8^+$ $BTLA^+$ subset in controlling disease in patients.

Downloaded from clincancerres.aacrjournals.org on October 21, 2020. © 2017 American Association for Cancer Research.

Published OnlineFirst July 28, 2017; DOI: 10.1158/1078-0432.CCR-16-1217

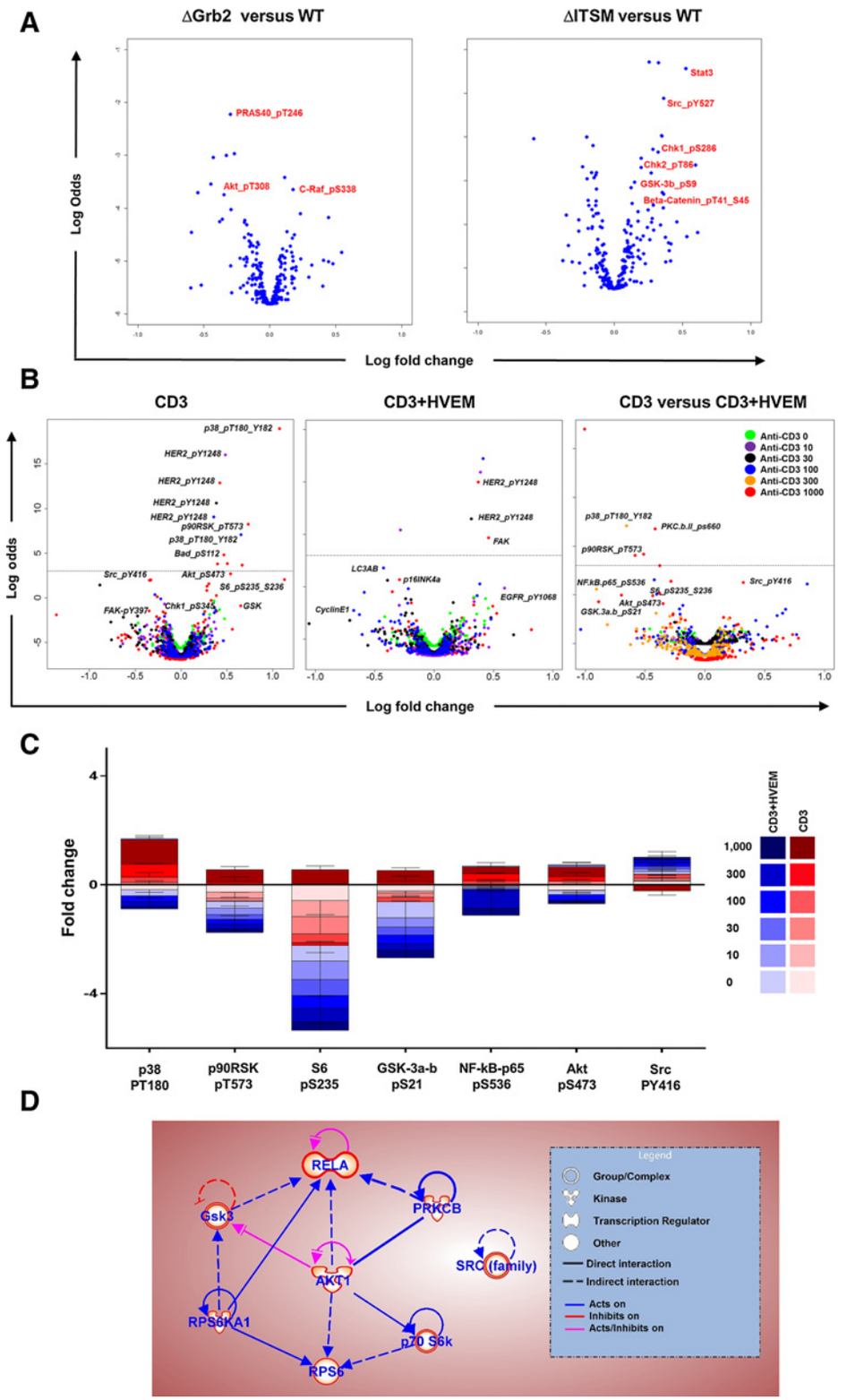

Figure 6.
BTLA-HVEM signaling axis suppresses MAPK, Akt, and NFκB pathways, but selectively augments the Src pathway. **A,** OT-1 BTLA KO T cells overexpressing WT BTLA or its variants were restimulated with plate-bound anti-CD3 and HVEM-Fc for 8 hours prior to harvest. Cells were lysed and the protein supernatant was collected to perform RPPA. Volcano plots depict fold change of proteins with the following comparisons: ΔGrb2 versus WT (left), ΔITSM versus WT (middle), and ΔITSM versus EM (right). Data shown represent two independent experiments. $P < 0.05$. P values were calculated using Linear models and empirical Bayes methods. **B** and **C,** Sorted CD8$^+$BTLA$^+$ TIL were stimulated with plate-bound anti-CD3 (0, 10, 30, 100, 300, and 1,000 ng/mL) alone or with HVEM-Fc for 8 hours prior to harvest. Cells were lysed and the protein supernatant was collected to perform RPPA. **B,** Volcano plot depicts fold change of proteins in CD8$^+$BTLA$^+$TIL upon T-cell activation with anti-CD3 alone (left), anti-CD3 + HVEM (middle), and anti-CD3 in comparison with anti-CD3 + HVEM (right). **C,** Bar graph demonstrates proteins that significantly change in comparison between anti-CD3 activation alone (red) and anti-CD3 + HVEM ligation (blue). **D,** Signaling network from the proteins that significantly change in **C** were clustered by Ingenuity Pathway Analysis. $N = 5$, $P < 0.05$. P values were calculated using Linear models and empirical Bayes methods.

The use of a single-cell nanowell-based cytolytic assay helped elucidate fundamental differences between the two subsets. Importantly, the results demonstrated that both subsets efficiently kill a first target, but the CD8$^+$BTLA$^+$ subset is more likely to survive after this killing event and kill another target, thus providing a rationale for the improved *in vivo* efficacy of the CD8$^+$BTLA$^+$ TILs.

Downloaded from clincancerres.aacrjournals.org on October 21, 2020. © 2017 American Association for Cancer Research.

Published OnlineFirst July 28, 2017; DOI: 10.1158/1078-0432.CCR-16-1217

The defective recall response seen in BTLA KO antigen-specific T-cell *in vivo* models used contrasts with previous literature. A publication by Krieg and colleagues evaluates the response of the $CD8^+$ BTLA-KO OT-1 T cells in a vaccination model and claims that there is more efficient memory formation in the BTLA-KO OT-1 T cells than their WT counterpart (30). This claim is based on the fact that there are twice as many $CD8^+$ OT-1 BTLA-KO T cells than WT counterpart in the spleen 30 days after the primary stimulation even though the BTLA-KO OT-1 subset peaked at lower frequency in the early days of the primary response. The BTLA-KO OT-1 also had a slightly lower fold expansion early (day 4) during the secondary expansion (7-fold vs. 10-fold) following boosting with peptide-pulsed DC. This is in contrast with the data obtained when boosting with an infectious agent expressing OVA, LM-OVA, where the BTLA-KO OT-1 expand more than the BTLA WT OT-1 at day 5 (91-fold vs. 191 fold). Unfortunately the experiment was not carried out longer. The authors conclude that BTLA KO OT-1 can form memory, and that the amplitude of the recall response may depend on the type of antigenic challenge used. Interestingly, another study utilizing BTLA KO animals and LM-OVA infection concluded that HVEM expression on T cells transduces a survival signal through interaction with BTLA expressed on other cells in the host and that interaction was required for $CD8^+$ T-cell memory generation (31).

There are a few key differences between our vaccination model and the reported studies. First of all, the adoptive cell transfer in the article by Krieg and colleagues is performed to allow competition between the cell subsets in the host. The authors actually transfer both BTLA WT OT-1 and BTLA KO OT-1 T cells at a 1:1 ratio to BTLA WT hosts and vaccinate the animals one day later with peptide-pulsed dendritic cells. While these experiments were designed to test BTLA's function, the known expression of BTLA's receptor, HVEM, on activated T cells, and its ability to transduce a survival signal by interactions in *trans* may become a confounding factor. In this system, it is possible that BTLA expressed on BTLA WT OT-1 may have interacted with HVEM on both transferred subsets which could have delivered a survival signal potent enough to limit the contraction phase and enhance memory formation for both subsets. The amplitude of the memory generation in this system could be controlled by the strength of TCR signal which clearly will be stronger in BTLA KO OT-1 as all studies are in agreement that BTLA suppresses TCR signaling.

Our experiments were designed to study the response of the two subsets separately, in different animals. Our data rather shows BTLA-mediated survival of T cells following effector function, probably due to dampening of TCR signaling and prevention of AICD. We believe that BTLA acts as a rheostat reducing TCR signaling during strong or chronic antigenic stimulation while also promoting cell survival due to the presence of both activating and inhibitory signaling motifs in its intracellular signaling domain. Our vaccination was administered by injection of the cognate peptide and anti-CD40 in saline subcutaneously, with topical application of the TLR 7 agonist imiquimod on the injection site and IP IL-2. This vaccination strategy, optimized by our collaborator Drs. Hailemichael and Overwijk, results in a powerful activation of the antigen-specific T-cell response (28). This stimulation produces a robust recall response in WT OT-1 and Pmel T cells; however, in our hands the BTLA KO OT-1 cells have a reduced ability to generate a recall response and Pmel BTLA KO cannot recall at all. We reasoned that BTLA expression may be essential to suppress overstimulation conducive to AICD and allow the survival of cells to form a memory pool. The method employed to vaccinate in the study by Krieg and colleagues, the use of peptide-pulsed DCs, may also not cause as much AICD as the stimulation used in our system, thus not requiring dampening of TCR stimulation by BTLA for survival.

We have demonstrated previously that resting $CD8^+BTLA^+$TIL manifested enhanced mitochondrial function and spare respiratory capacity (SRC) as compared with their $CD8^+BTLA^-$ TIL counterpart (32). High SRC has been reported to be a feature of memory $CD8^+$ T cells distinguishing them from naïve and effector subsets, and was found to play a role in survival of the memory $CD8^+$ subset conducive to the establishment of a long-lived memory pool (33). Our findings of the better survival of the $CD8^+BTLA^+$ TIL subset after a killing event are consistent with a prosurvival advantage. A recent study indicated that increased SRC was strongly associated with a superior bioenergetic capacity, which helped improve T-cell survival and motility under hypoxic conditions (34). The intrinsic properties of this subset provide an intriguing possibility for why infusion of large numbers of $CD8^+BTLA^+$TILs positively correlates with clinical response to TIL ACT in metastatic melanoma patients.

We have found that a BTLA-dependent potentiation of IL-2 secretion entirely depends on Grb2 motif. Disruption of the ITIM and ITSM motifs did not alter the levels of IL-2 induced by BTLA, suggesting a signaling pathway independent of the proinhibitory influence of ITIM and ITSM. Our findings are consistent with previous reports that have shown that Grb2-linked SLP-76 and Vav interaction are involved in IL-2 production, and that recruitment of Grb2 is essential for CD28-induced IL-2 production (19, 35, 36). Our current study reveals that BTLA engagement in the context of TCR stimulation results in IL-2 production in a manner similar to CD28 which positions BTLA as both a coinhibitory and costimulatory molecule. The *in vivo* relevance of BTLA-dependent IL-2 production in the context of T-cell activation warrants further study. Autocrine IL-2 production by $CD8^+$ T cells has been shown to be essential for secondary expansion of $CD8^+$ memory T cells which could potentially explain the lack of secondary expansion seen in BTLA KO cells after boosting with the vaccinating antigen (37). The prosurvival properties conferred by BTLA on $CD8^+$ T cells may come from the interaction of BTLA with HVEM on activated T cells as it was demonstrated for $CD4^+$ murine T cells (38, 39). However, the HVEM interaction with its alternative ligand LIGHT rather than BTLA has been implicated in furthering $CD4^+$ T-cell activation and survival (39). In our experiments, the absence of BTLA may render HVEM available to bind to its alternative ligand LIGHT to provide costimulatory signaling to T cells; however, this mechanism was not sufficient to rescue the establishment of memory cells able to respond to a recall antigen stimulation.

Conversely, we did not observe any major differences in *in vitro* killing capacity and cytotoxic cytokine production between BTLA KO T cells versus BTLA KO T cells overexpressing BTLA WT or its mutants. This suggests that BTLA signaling does not affect tumor killing capability. Our findings are consistent with the previous report showing that the BTLA blockade in γδT cells had no effect on the tumor lysis (40).

We did not observe a significant impact of WT BTLA when the molecule was reintroduced in BTLA KO T cells. However, malfunction of ITIM and ITSM motifs significantly enhanced T cell proliferation while Grb2 alteration reduced the proliferation. A lack of impact of BTLA on $CD4^+$ T-cell proliferative response has

Downloaded from clincancerres.aacrjournals.org on October 21, 2020. © 2017 American Association for Cancer Research.

Published OnlineFirst July 28, 2017; DOI: 10.1158/1078-0432.CCR-16-1217

been reported previously (12). Previous studies in both human and mouse settings indicated that CD8$^+$ T cells were intrinsically less susceptible to BTLA-mediated inhibition as compared with CD4$^+$ T cells (9, 41). This might explain the minimal inhibition of WT as compared with EM in CD8$^+$ T cells in terms of proliferation.

We noticed that the Akt signaling pathway was remarkably attenuated in BTLA ΔGrb2, while the phosphorylation of Src was enhanced in BTLA ΔITSM. This finding is consistent with a previous report demonstrating that ITIM and ITSM motifs of PD-1 inhibited signals through Akt and MAPK (10). However, in the presence of costimulation mediated through the BTLA Grb2 motif, as in the case of ΔITIM/ITSM, the phosphorylation of Akt was unaltered, suggesting that Grb2 is not directly involved in maintaining or augmenting Akt phosphorylation. Taken together, these data suggests that the Akt pathway in BTLA was likely targeted by SHP1/2, similar to what was found in PD-1.

Overexpression of Grb2 in osteoclasts was shown to promote phosphorylation of Src at Y416 and the opposite result was obtained when Grb2 expression was disrupted (42). From our data, it is clear that the phosphorylation of Src increased when Grb2 was providing BTLA signaling in the absence of functional ITIM and ITSM motifs. This could result from either the direct effect of Grb2 signal transduction or the lack of dephosphorylation normally caused by SHP1/2 via ITIM and ITSM motifs. As the phosphorylation of Src is not significantly influenced by the ITIM/ITSM cosignaling (ΔGrb2), we conclude that it is likely to be Grb2-mediated Src activation.

Our data of BTLA signaling in mouse T cells was found to be consistent with changes observed when activated human CD8$^+$BTLA$^+$TILs were costimulated by HVEM. Indeed, we observed an attenuation of MAPK, NFκB, and Akt signaling proteins, but phosphorylation of Src was enhanced when human TILs were stimulated with anti-CD3 and HVEM as compared with CD3 alone. This suggested that the downstream signaling pathway of BTLA in mice and humans possibly share similar downstream signaling targets.

Overall, our study sheds light on a dual role of BTLA as both a costimulatory and coinhibitory molecule. This observation is supported by a study reporting that the gene expression profile of CD4$^+$ T cells activated with CD3 and BTLA engagement mimics the profile induced by costimulatory molecules (12). In our hands, the integration of the positive and negative signals transduced by BTLA promotes IL-2 secretion while reducing effector cytokine production and proliferation in certain contexts. In addition, the inherent properties of the less-differentiated T cells expressing BTLA also display enhanced resistance to apoptosis and an efficient bioenergetic profile providing a survival advantage following tumor killing. These findings support the concept that the intrinsic attribute of the less-differentiated CD8$^+$BTLA$^+$ human TIL subset together with balanced signals transduced by the engagement of HVEM in the tumor microenvironment on melanoma cells could provide a costimulatory signal to CD8$^+$BTLA$^+$ TILs promoting IL-2 secretion, T-cell survival, and antitumor function.

Disclosure of Potential Conflicts of Interest

No potential conflicts of interest were disclosed.

Authors' Contributions

Conception and design: K. Ritthipichai, C. Haymaker, L.G. Radvanyi, P. Hwu, C. Bernatchez

Development of methodology: K. Ritthipichai, L.G. Radvanyi

Acquisition of data (provided animals, acquired and managed patients, provided facilities, etc.): K. Ritthipichai, W.W. Overwijk, L. Vence, N. Varadarajan

Analysis and interpretation of data (e.g., statistical analysis, biostatistics, computational analysis): K. Ritthipichai, C. Haymaker, M. Martinez-Paniagua, A. Aschenbrenner, W.W. Overwijk, L. Vence, J. Roszik, N. Varadarajan, L.G. Radvanyi, P. Hwu, C. Bernatchez

Writing, review, and/or revision of the manuscript: K. Ritthipichai, C. Haymaker, M. Martinez-Paniagua, A. Aschenbrenner, W.W. Overwijk, J. Roszik, N. Varadarajan, P. Hwu, C. Bernatchez

Administrative, technical, or material support (i.e., reporting or organizing data, constructing databases): X. Yi, M. Zhang, C. Kale, Y. Hailemichael

Study supervision: R. Nurieva, L.G. Radvanyi, C. Bernatchez

Acknowledgments

The authors thank the melanoma surgical staff at MD Anderson Cancer Center. We appreciate help from TIL laboratory for processing tumor samples. We are thankful for the staff at the MD Anderson Cancer Center Flow Cytometry Core Facility for technical assistance with cell sorting. We are grateful to Drs. Weiyi Peng and Ondrej Havranek for guidance on experimental design.

Grant Support

This work was supported by the National Cancer Institute (NCI) grants R01-CA111999 (to P. Hwu), R01CA174385 (to N. Varadarajan) and 1R21CA178580-01 (to C. Bernatchez). STR DNA fingerprinting was done by the CCSG-funded Characterized Cell Line Core at MD Anderson, NCI grant P30CA016672. This grant also supported the the Flow Cytometry Core Facility that was used for cell sorting and the Functional Proteomics Reverse Phase Protein Array (RPPA) Core. This work was further supported by the UT Health Innovation for Cancer Prevention Research Pre-doctoral Fellow, The UT School of Public Health-Cancer Prevention and Research Institute of Texas grant RP160015 (to K. Ritthipichai and A. Aschenbrenner), RP130570 to (N. Varadarajan), RP140522 (to W.W. Overwijk), NIH grant A1R03AI120027 and 1R21AI20012 (to R. Nurieva) and the Dr. Miriam and Sheldon G. Adelson Medical Research Foundation (AMRF), Melanoma Research Alliance Young Investigator Award (509800; to N. Varadarajan), and the Mulva Foundation.

The costs of publication of this article were defrayed in part by the payment of page charges. This article must therefore be hereby marked *advertisement* in accordance with 18 U.S.C. Section 1734 solely to indicate this fact.

Received May 16, 2016; revised January 29, 2017; accepted July 19, 2017; published OnlineFirst July 28, 2017.

References

1. Dudley ME, Wunderlich JR, Yang JC, Sherry RM, Topalian SL, Restifo NP, et al. Adoptive cell transfer therapy following non-myeloablative but lymphodepleting chemotherapy for the treatment of patients with refractory metastatic melanoma. J Clin Oncol 2005;23:2346–57.
2. Besser MJ, Shapira-Frommer R, Treves AJ, Zippel D, Itzhaki O, Hershkovitz L, et al. Clinical responses in a phase II study using adoptive transfer of short-term cultured tumor infiltration lymphocytes in metastatic melanoma patients. Clin Cancer Res 2010;16:2646–55.
3. Pilon-Thomas S, Kuhn L, Ellwanger S, Janssen W, Royster E, Marzban S, et al. Efficacy of adoptive cell transfer of tumor-infiltrating lymphocytes after lymphopenia induction for metastatic melanoma. J Immunother 2012;35:615–20.
4. Radvanyi LG, Bernatchez C, Zhang M, Fox PS, Miller P, Chacon J, et al. Specific lymphocyte subsets predict response to adoptive cell therapy using expanded autologous tumor-infiltrating lymphocytes in metastatic melanoma patients. Clin Cancer Res 2012;18:6758–70.

Downloaded from clincancerres.aacrjournals.org on October 21, 2020. © 2017 American Association for Cancer Research.

Published OnlineFirst July 28, 2017; DOI: 10.1158/1078-0432.CCR-16-1217

5. Watanabe N, Gavrieli M, Sedy JR, Yang J, Fallarino F, Loftin SK, et al. BTLA is a lymphocyte inhibitory receptor with similarities to CTLA-4 and PD-1. Nat Immunol 2003;4:670–9.
6. Sedy JR, Gavrieli M, Potter KG, Hurchla MA, Lindsley RC, Hildner K, et al. B and T lymphocyte attenuator regulates T cell activation through interaction with herpesvirus entry mediator. Nat Immunol 2005;6:90–8.
7. Gavrieli M, Watanabe N, Loftin SK, Murphy TL, Murphy KM. Characterization of phosphotyrosine binding motifs in the cytoplasmic domain of B and T lymphocyte attenuator required for association with protein tyrosine phosphatases SHP-1 and SHP-2. Biochem Biophys Res Commun 2003; 312:1236–43.
8. Chemnitz JM, Lanfranco AR, Braunstein I, Riley JL. B and T lymphocyte attenuator-mediated signal transduction provides a potent inhibitory signal to primary human CD4 T cells that can be initiated by multiple phosphotyrosine motifs. J Immunol 2006;176:6603–14.
9. Otsuki N, Kamimura Y, Hashiguchi M, Azuma M. Expression and function of the B and T lymphocyte attenuator (BTLA/CD272) on human T cells. Biochem Biophys Res Commun 2006;344:1121–7.
10. Patsoukis N, Brown J, Petkova V, Liu F, Li L, Boussiotis VA. Selective effects of PD-1 on Akt and Ras pathways regulate molecular components of the cell cycle and inhibit T cell proliferation. Sci Signal 2012;5:ra46.
11. Gavrieli M, Murphy KM. Association of Grb-2 and PI3K p85 with phosphotyrosile peptides derived from BTLA. Biochem Biophys Res Commun 2006;345:1440–5.
12. Wakamatsu E, Mathis D, Benoist C. Convergent and divergent effects of costimulatory molecules in conventional and regulatory CD4+ T cells. Proc Natl Acad Sci U S A 2013;110:1023–8.
13. Legat A, Speiser DE, Pircher H, Zehn D, Fuertes Marraco SA. Inhibitory receptor expression depends more dominantly on differentiation and activation than "Exhaustion" of human CD8 T cells. Front Immunol 2013;4:455.
14. Haymaker CL, Wu RC, Ritthipichai K, Bernatchez C, Forget MA, Chen JQ, et al. BTLA marks a less-differentiated tumor-infiltrating lymphocyte subset in melanoma with enhanced survival properties. Oncoimmunology 2015;4:e1014246.
15. Gattinoni L, Lugli E, Ji Y, Pos Z, Paulos CM, Quigley MF, et al. A human memory T cell subset with stem cell-like properties. Nat Med 2011; 17:1290–7.
16. Wang X, Berger C, Wong CW, Forman SJ, Riddell SR, Jensen MC. Engraftment of human central memory-derived effector CD8+ T cells in immunodeficient mice. Blood 2011;117:1888–98.
17. Berger C, Jensen MC, Lansdorp PM, Gough M, Elliott C, Riddell SR. Adoptive transfer of effector CD8+ T cells derived from central memory cells establishes persistent T cell memory in primates. J Clin Invest 2008;118:294–305.
18. Hinrichs CS, Borman ZA, Gattinoni L, Yu Z, Burns WR, Huang J, et al. Human effector CD8+ T cells derived from naive rather than memory subsets possess superior traits for adoptive immunotherapy. Blood 2011;117:808–14.
19. Wu J, Motto DG, Koretzky GA, Weiss A. Vav and SLP-76 interact and functionally cooperate in IL-2 gene activation. Immunity 1996;4:593–602.
20. Li Y, Liu S, Hernandez J, Vence L, Hwu P, Radvanyi L. MART-1-specific melanoma tumor-infiltrating lymphocytes maintaining CD28 expression have improved survival and expansion capability following antigenic restimulation in vitro. J Immunol 2010;184:452–65.
21. Nanjundan M, Byers LA, Carey MS, Siwak DR, Raso MG, Diao L, et al. Proteomic profiling identifies pathways dysregulated in non-small cell lung cancer and an inverse association of AMPK and adhesion pathways with recurrence. J Thorac Oncol 2010;5:1894–904.
22. Smyth GK. Linear models and empirical bayes methods for assessing differential expression in microarray experiments. Stat Appl Genet Mol Biol 2004;3:Article3.
23. Liadi I, Roszik J, Romain G, Cooper LJ, Varadarajan N. Quantitative high-throughput single-cell cytotoxicity assay for T cells. J Vis Exp 2013:e50058.
24. Cancer Genome Atlas Network. Genomic classification of cutaneous melanoma. Cell 2015;161:1681–96.
25. Klebanoff CA, Scott CD, Leonardi AJ, Yamamoto TN, Cruz AC, Ouyang C, et al. Memory T cell-driven differentiation of naive cells impairs adoptive immunotherapy. J Clin Invest 2016;126:318–34.
26. Liadi I, Singh H, Romain G, Rey-Villamizar N, Merouane A, Adolacion JR, et al. Individual motile CD4(+) T cells can participate in efficient multikilling through conjugation to multiple tumor cells. Cancer Immunol Res 2015;3:473–82.
27. Romain G, Senyukov V, Rey-Villamizar N, Merouane A, Kelton W, Liadi I, et al. Antibody Fc engineering improves frequency and promotes kinetic boosting of serial killing mediated by NK cells. Blood 2014;124: 3241–9.
28. Hailemichael Y, Dai Z, Jaffarzad N, Ye Y, Medina MA, Huang XF, et al. Persistent antigen at vaccination sites induces tumor-specific CD8(+) T cell sequestration, dysfunction and deletion. Nat Med 2013;19:465–72.
29. Kovacina KS, Park GY, Bae SS, Guzzetta AW, Schaefer E, Birnbaum MJ, et al. Identification of a proline-rich Akt substrate as a 14-3-3 binding partner. J Biol Chem 2003;278:10189–94.
30. Krieg C, Boyman O, Fu YX, Kaye J. B and T lymphocyte attenuator regulates CD8+ T cell-intrinsic homeostasis and memory cell generation. Nat Immunol 2007;8:162–71.
31. Steinberg MW, Huang Y, Wang-Zhu Y, Ware CF, Cheroutre H, Kronenberg M. BTLA interaction with HVEM expressed on CD8(+) T cells promotes survival and memory generation in response to a bacterial infection. PLoS One 2013;8:e77992.
32. Forget MA, Haymaker C, Dennison JB, Toth C, Maiti S, Fulbright OJ, et al. The beneficial effects of a gas-permeable flask for expansion of Tumor-Infiltrating lymphocytes as reflected in their mitochondrial function and respiration capacity. Oncoimmunology 2015;5:e1057386.
33. van der Windt GJ, Everts B, Chang CH, Curtis JD, Freitas TC, Amiel E, et al. Mitochondrial respiratory capacity is a critical regulator of CD8+ T cell memory development. Immunity 2012;36:68–78.
34. Dimeloe S, Mehling M, Frick C, Loeliger J, Bantug GR, Sauder U, et al. The immune-metabolic basis of effector memory CD4+ T cell function under hypoxic conditions. J Immunol 2016;196:106–14.
35. Jackman JK, Motto DG, Sun Q, Tanemoto M, Turck CW, Peltz GA, et al. Molecular cloning of SLP-76, a 76-kDa tyrosine phosphoprotein associated with Grb2 in T cells. J Biol Chem 1995;270:7029–32.
36. Harada Y, Ohgai D, Watanabe R, Okano K, Koiwai O, Tanabe K, et al. A single amino acid alteration in cytoplasmic domain determines IL-2 promoter activation by ligation of CD28 but not inducible costimulator (ICOS). J Exp Med 2003;197:257–62.
37. Feau S, Arens R, Togher S, Schoenberger SP. Autocrine IL-2 is required for secondary population expansion of CD8(+) memory T cells. Nat Immunol 2011;12:908–13.
38. Cheung TC, Steinberg MW, Oborne LM, Macauley MG, Fukuyama S, Sanjo H, et al. Unconventional ligand activation of herpesvirus entry mediator signals cell survival. Proc Natl Acad Sci U S A 2009;106:6244–9.
39. Soroosh P, Doherty TA, So T, Mehta AK, Khorram N, Norris PS, et al. Herpesvirus entry mediator (TNFRSF14) regulates the persistence of T helper memory cell populations. J Exp Med 2011;208:797–809.
40. Gertner-Dardenne J, Fauriat C, Orlanducci F, Thibult ML, Pastor S, Fitzgibbon J, et al. The co-receptor BTLA negatively regulates human Vgamma9Vdelta2 T-cell proliferation: a potential way of immune escape for lymphoma cells. Blood 2013;122:922–31.
41. Krieg C, Han P, Stone R, Goularte OD, Kaye J. Functional analysis of B and T lymphocyte attenuator engagement on CD4+ and CD8+ T cells. J Immunol 2005;175:6420–7.
42. Levy-Apter E, Finkelshtein E, Vemulapalli V, Li SS, Bedford MT, Elson A. Adaptor protein GRB2 promotes Src tyrosine kinase activation and podosomal organization by protein-tyrosine phosphatase in osteoclasts. J Biol Chem 2014;289:36048–58.

Downloaded from clincancerres.aacrjournals.org on October 21, 2020. © 2017 American Association for Cancer Research.

Published OnlineFirst July 28, 2017; DOI: 10.1158/1078-0432.CCR-16-1217

AACR American Association for Cancer Research

Clinical Cancer Research

Multifaceted Role of BTLA in the Control of CD8$^+$ T-cell Fate after Antigen Encounter

Krit Ritthipichai, Cara L. Haymaker, Melisa Martinez, et al.

Clin Cancer Res 2017;23:6151-6164. Published OnlineFirst July 28, 2017.

Updated version	Access the most recent version of this article at: doi:10.1158/1078-0432.CCR-16-1217
Supplementary Material	Access the most recent supplemental material at: http://clincancerres.aacrjournals.org/content/suppl/2017/07/28/1078-0432.CCR-16-1217.DC1

Cited articles	This article cites 41 articles, 20 of which you can access for free at: http://clincancerres.aacrjournals.org/content/23/20/6151.full#ref-list-1
Citing articles	This article has been cited by 4 HighWire-hosted articles. Access the articles at: http://clincancerres.aacrjournals.org/content/23/20/6151.full#related-urls

E-mail alerts	Sign up to receive free email-alerts related to this article or journal.
Reprints and Subscriptions	To order reprints of this article or to subscribe to the journal, contact the AACR Publications Department at pubs@aacr.org.
Permissions	To request permission to re-use all or part of this article, use this link http://clincancerres.aacrjournals.org/content/23/20/6151. Click on "Request Permissions" which will take you to the Copyright Clearance Center's (CCC) Rightslink site.

Downloaded from clincancerres.aacrjournals.org on October 21, 2020. © 2017 American Association for Cancer Research.